Predicting Elastic Properties of Unidirectional SU8/ZnO Nanocomposites using COMSOL Multiphysics

Neelam Mishra[1], and Kaushik Das[*1]
[1]School of Minerals Metallurgical and Materials Engineering, Indian Institute of Technology Bhubaneswar
*Corresponding author: Room 606, Block A1, Toshali Bhawan, SMMME, IIT Bhubaneswar, Bhubaneswar 751007, India, kaushik@iitbbs.ac.in

Abstract: In this work the effective elastic properties of a SU8 photoresist matrix reinforced with ZnO nanomaterial (in the form of cylindrical nanowires, spherical and ellipsoidal particles) have been evaluated employing COMSOL Multiphysics®. The Solid Mechanics Physics of Structural Mechanics module is used in this work for the stationary study of three-dimensional representative volume elements. Effective elastic properties of the composite such as longitudinal elastic modulus (E_1), transverse elastic modulus (E_2), axial shear modulus (G_{12}), and transverse shear modulus (G_{23}) are obtained by employing homogeneous displacement boundary conditions for different volume fractions of reinforcement material ranging from zero to a maximum of 0.7. The effect of various parameters such as volume fraction, continuity, and shape of the reinforcement on the effective elastic properties of the nanocomposite are presented.

Keywords: nanocomposites, effective properties, representative volume element (RVE)

1. Introduction

Integration of nanomaterials in the form of nanoparticles and/or nanowires to microsystems technologies can lead to a new generation of devices with novel functionalities. One way to integrate nanomaterials with MEMS is by using nanocomposites as structural components of these devices. A nanocomposite consisting of a negative photoresist SU8 as the matrix, and zinc oxide (ZnO), a piezoelectric nanomaterial (in the form of nanowires, and/or nanoparticles) as the reinforcement, is a promising candidate for applications in energy-harvesting microdevices [1]. Proper design of the micro/nanodevices requires the knowledge of the effective material properties of the nanocomposite. The properties of interest are the effective elastic properties and the effective dielectric properties of the polymer/ZnO composite. As a first step towards predicting the effective properties of a piezoelectric composite, in this work an effort has been made to calculate the effective elastic properties of a SU8/ZnO composite, using finite element method (FEM).

Prediction of effective properties of composites using FEM method is an active area of research. Sun and Vaidya established a micromechanics-based foundation for predicting the effective properties of unidirectional composites by performing finite element analysis of representative volume elements (RVEs) [2]. Boundary conditions in the form of homogeneous displacement, homogeneous traction, and periodic boundary conditions have been applied to RVEs to evaluate teir effective properties [3]. Appropriate unit cells and corresponding homogeneous boundary conditions have been identified by Li for the finite element analysis of unidirectional periodic composites [4, 5]. In this study, homogeneous displacement boundary conditions have been employed on a cubic RVE to evaluate effective properties of unidirectional composites. COMSOL Multiphysics is used due to the ease of applying boundary conditions.

This manuscript is organized in the following fashion. Section 2 discusses the theory of linear elasticity, as applicable for heterogeneous materials. The RVE is introduced, and boundary conditions required for the estimation of elastic properties are described explicitly in section 3. Section 4 lists the material properties of the constituent phases. The variation of the effective elastic properties of the composite as a function of volume fraction of the reinforcement phase is presented in section 5.

2. Theory

According to the theory of linear elasticity, the interaction between the stress field and the strain field of a homogeneous material can be

expressed by the following constitutive relationship:

$$\sigma_{ij} = C_{ijkl}\varepsilon_{kl}. \quad (1)$$

Here σ is the stress tensor, ε is the strain tensor, and C is the fourth order stiffness tensor, and the indices i, j, k, and l range from 1-3. However, in general, materials such as composites are heterogeneous. One can relate the volume averaged stress field ($\bar{\sigma}$) of a heterogeneous material to the volume averaged strain field ($\bar{\varepsilon}$) by the effective stiffness tensor C^{eff} i.e.

$$\bar{\sigma}_{ij} = C^{eff}_{ijkl}\bar{\varepsilon}_{kl} \quad (2)$$

For a composite, the effective stiffness tensor is a function of the elastic properties, geometry, orientation and spatial distribution of the constituent phases. Several micromechanical approaches have been developed for predicting effective properties of composites using information of the individual constituents. Most notable among these approaches is the Eshelby-Mori-Tanaka approach [6], where the stress/strain fields in the constituent phases are considered to be uniform. Moreover, these approaches are unable to take into account complicated geometries and the spatial distribution of the reinforcement phases. On the other hand, approaches based on finite element method provide a more realistic prediction of the effective properties by taking into account the geometries of the constituent phases and the non-uniform stress/strain fields in the constituent phases. The first step towards prediction of effective properties of composites is to select an appropriate a representative volume element or a unit cell. This representative volume element must be large enough to contain all microstructural information but should be small enough compared to the structure under study. Using FEM the volume-averaged stresses and strains can be calculated as

$$\overline{\sigma_{ij}} = \frac{1}{V}\int \sigma_{ij}dV = \frac{1}{V}\sum_{n=1}^{nel}\sigma_{ij}^{(n)}V^{(n)} \quad (3)$$

$$\overline{\varepsilon_{ij}} = \frac{1}{V}\int \varepsilon_{ij}dV = \frac{1}{V}\sum_{n=1}^{nel}\varepsilon_{ij}^{(n)}V^{(n)} \quad (4)$$

In equations (3) - (4), V is the volume of the RVE, *nel* is total number of finite elements in the RVE, $V^{(n)}$ is the volume of the n^{th} element, σ is ij^{th} component of the stress tensor calculated in the n^{th} element, and $\varepsilon_{ij}^{(n)}$ is ij^{th} component of the strain tensor calculated in the n^{th} element. Boundary conditions are applied on the surfaces of the RVE. In the case of a cubic RVE there would be six sets of boundary conditions. For homogeneous applied strain (ε_{ij}^0), the boundary conditions applied on the surfaces of the cube are of the form $u_i = \varepsilon_{ij}^0 x_j$, where x_j refers to the coordinates of the surfaces of the RVE. The components of the strain tensor, ε_{ij} are related to the displacements (u by –

The calculation of the effective elastic properties of the composite is performed from the values of $\bar{\sigma}_{ij}$ and $\bar{\varepsilon}_{ij}$ calculated under appropriate boundary conditions. The boundary conditions applied on the RVE to calculate effective axial modulus (E_1), effective transverse modulus (E_2), effective axial shear modulus (G_{12}), and effective transverse shear modulus (G_{23}) are presented in the next section.

3. RVE and Boundary Conditions

A discussion of boundary conditions requires a description of the RVEs. All RVEs considered in this study are cubic in shape, with cube-edge ($2a$) of 120 nm. The origin of the coordinate system, and the centroid of the reinforcement coincide with the centroid of the cube. There are three mutually orthogonal mirror planes through the centre of the RVE. Four different types of RVEs based on the geometry and continuity of reinforcements are considered in this study. All composites considered in this study are unidirectional. RVE1 represents a continuous nanorod composite, while RVE2 represents a discontinuous composite reinforced with long cylindrical ZnO nanorods with aspect ratio (length:diamter) of 1.2:1. RVE3 represents a spherical ZnO nanoparticle reinforced composite, and RVE4 represents a composite reinforced with ellipsoidal ZnO nanoparticle. Figure 1 shows the RVEs considered in this study. Due to the symmetric geometries of the RVEs, only one-eighth of the full RVEs are needed for the finite element analysis. The boundaries of the reduced structures are:

B_1: $x = 0,\ 0 \le y \le a,\ 0 \le z \le a$, $\mathbf{n}$ = (-1, 0, 0)

B_2: $x = +a,\ 0 \le y \le a,\ 0 \le z \le a$, $\mathbf{n}$ = (1, 0, 0)

B_3: $y = 0,\ 0 \le x \le a,\ 0 \le z \le a$, $\mathbf{n}$ = (0, -1, 0)

B_4: $y = +a,\ 0 \le x \le a,\ 0 \le z \le a$, $\mathbf{n}$ = (0, 1, 0)

B_5: $z = 0,\ 0 \le x \le a,\ 0 \le y \le a$, $\mathbf{n}$ = (0, 0, -1)

B_6: $z = +a,\ 0 \le x \le a,\ 0 \le y \le a$, $\mathbf{n}$ = (0, 0, 1)

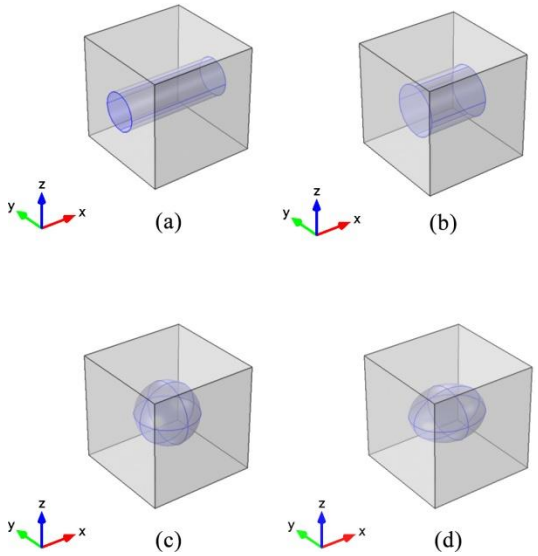

Figure 1. Images of full unidirectional RVEs: (a) RVE1 for a continuous composite with cylindrical reinforcement; (b) RVE2 for a discontinuous composite with cylindrical reinforcement, and the ratio of length to diameter is 1.2:1; (c) RVE3 for a discontinuous composite with a spherical reinforcement; (d) RVE4 for a discontinuous composite with an ellipsoid as the reinforcement, and the semi-axes are in the ratio of 1.5:1.25:1;

Here, **n** represents the normal vector to the corresponding boundary. The components of the vector along x, y and z directions are provided in within brackets. The boundary conditions for the prediction of effective elastic properties of the composite are provided in table 1. Here ε_0 is the applied strain, while $\bar{\varepsilon}_{11}$, $\bar{\varepsilon}_{22}$, and $\bar{\varepsilon}_{33}$ are unknown volume-averaged normal strains which should be left free. This is accomplished in COMSOL Multiphysics using the following procedure.

First, a volume integration operator, intop1 is defined for the entire domain. Next, the volume averaged unknown strains are calculated as:

$$\bar{\varepsilon}_{11} = \frac{1}{V}\int \varepsilon_{11} dV = \text{intop1(solid.eXX)/(a*a*a)} \quad (5)$$

Similarly,

$$\bar{\varepsilon}_{22} = \text{intop1(solid.eYY)/(a*a*a)} \quad (6)$$

and

$$\bar{\varepsilon}_{33} = \text{intop1(solid.eZZ)/(a*a*a)} \quad (7)$$

Here solid.eXX, solid.eYY and solid.eZZ are strains calculated in the global coordinate system.

The RVEs are meshed using tetrahedral elements, and the finite element model is solved using the iterative multigrid solver. Post-processing involves evaluation of volume-averaged stresses and strains. The effective properties can next be calculated using the following equations:

$$E_1 = \frac{\bar{\sigma}_{11}}{\bar{\varepsilon}_{11}} \quad (8)$$

$$E_2 = \frac{\bar{\sigma}_{22}}{\bar{\varepsilon}_{22}} \quad (9)$$

$$G_{12} = \frac{\bar{\sigma}_{12}}{2\bar{\varepsilon}_{12}} \quad (10)$$

$$G_{23} = \frac{\bar{\sigma}_{23}}{2\bar{\varepsilon}_{23}} \quad (11)$$

$$\nu_{12} = -\frac{\bar{\varepsilon}_{22}}{\bar{\varepsilon}_{11}} \quad (12)$$

$$\nu_{23} = -\frac{\bar{\varepsilon}_{33}}{\bar{\varepsilon}_{22}} \quad (13)$$

Table 1: Boundary conditions for evaluating the effective elastic properties

Property	B_1	B_2	B_3	B_4	B_5	B_6
E_1, ν_{12}	$u = 0$	$u = a\varepsilon_0$	$v = 0$	$v = a\bar{\varepsilon}_{22}$	$w = 0$	$w = a\bar{\varepsilon}_{33}$
E_2, ν_{23}	$u = 0$	$u = a\bar{\varepsilon}_{11}$	$v = 0$	$v = a\varepsilon_0$	$w = 0$	$w = a\bar{\varepsilon}_{33}$
G_{12}	$v = 0$ $w = 0$	$v = 0$ $w = 0$	$u = 0$ $w = 0$	$u = 2a\varepsilon_0$ $w = 0$	$w = 0$	$w = 0$
G_{23}	$u = 0$	$u = 0$	$u = 0$ $w = 0$	$u = 0$ $w = 0$	$u = 0$ $v = 0$	$u = 0$ $v = 2a\varepsilon_0$

4. Material Properties

The matrix, SU8 is considered to be isotropic, with Young's modulus, $E_{SU8} = 4.4\ GPa$, and Poisson's ratio $\nu_{SU8} = 0.22$ [7]. The reinforcement, ZnO is considered to have a wurtzite crystal structure, which is transversely isotropic. The plane of isotropy of ZnO is considered to be parallel to the *y*-*z* plane, while the *c*-axis of ZnO coincides with the *x*-axis of the global coordinate system. The coefficients of the stiffness matrix of ZnO is available in literature [8] where the *c*-axis of ZnO coincides with the *z*-axis of the global coordinate system. Hence, the resultant coefficients applicable in this study was obtained after appropriate coordinate transformations. Table 2 provides the coefficients of the stiffness matrices of SU8 and ZnO used in this work.

Table 2: Coefficients of the stiffness matrices of the constituent phases of the composite

Coefficient	SU8	ZnO
C_{11}	5.023 GPa	210.9 GPa
C_{12}	1.417 GPa	105.1 GPa
C_{13}	1.417 GPa	105.1 GPa
C_{23}	1.417 GPa	121.1 GPa
C_{33}	5.023 GPa	209.7 GPa
C_{44}	1.803 GPa	44.29 GPa
C_{55}	1.803 GPa	42.47 GPa
C_{66}	1.803 GPa	42.47 GPa

5. Results and Discussions

The effect of volume fraction of ZnO on the effective elastic properties of the SU8/ZnO nanocomposites are presented in this section. For RVE1, volume fraction increases by increasing the radius of the cylindrical reinforcement. The maximum volume fraction of reinforcement for RVE1 is ~0.78. In the case of RVE2, the reinforcement is in the form of a cylinder as well. However, the length:diameter ratio of the cylindrical reinforcement is maintained at 1.2:1 for all volume fractions. The maximum volume fraction for RVE2 is ~0.54. As mentioned earlier, RVE3 has a spherical reinforcement, and the maximum volume fraction is ~0.52. RVE4 has an ellipsoid with semi-axes ratio a:b:c = 1.5:1.25:1 as the reinforcement. The maximum volume fraction of reinforcement is limited to ~0.29. In this study for the ease of meshing, we have considered volume fractions in the range of 0 - 0.7 for RVE1, in the range of 0 - 0.52 for RVE2 and RVE3, and in the range of 0 - 0.26 for RVE4.

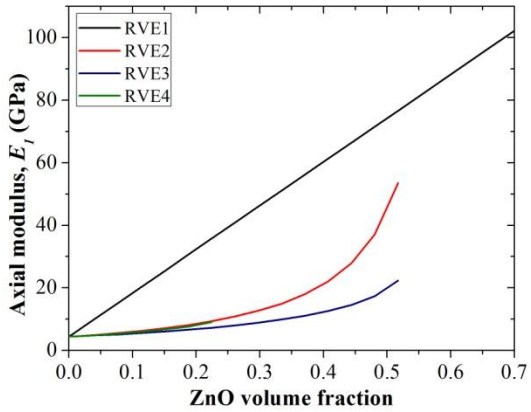

Figure 2. Variation of axial modulus as a function of volume fraction of ZnO.

Figure 2 shows the effect of volume fraction on the axial modulus of Su8/ZnO composites. It is observed that the continuous composite exhibits higher axial modulus compared to the discontinuous composites. Among the discontinuous composites, the composite reinforced with spherical particle exhibits the lowest axial modulus at any volume fraction in the range of 0 - 0.52. The discontinuous composites with cylindrical and ellipsoidal reinforcements have similar values for axial modulus at low volume fractions in the range of 0 - 0.26.

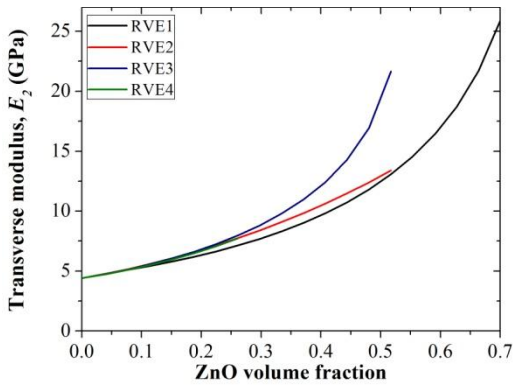

Figure 3. Variation of transverse modulus as a function of volume fraction of ZnO

Figure 3 shows the effect of volume fraction on the transverse modulus of SU8/ZnO composites. The continuous composite exhibit the least values of transverse modulus when compared to

the discontinuous composite. For low volume fractions in the range of 0 - 0.26, the values predicted for the discontinuous composites are similar. Beyond the volume fraction of ~0.26, the discontinuous composite with spherical reinforcement exhibit higher transverse modulus compared to the discontinuous composite with cylindrical reinforcement.

Figures 4 and 5 show the effect of volume fraction on the effective axial shear modulus and on the effective transverse shear modulus of the Su8/ZnO composites. The axial shear modulus is less sensitive to continuity and geometry of the reinforcement compared to the other effective elastic moduli. In the case of the transverse shear modulus, it is observed that composite with reinforcement in the form of spherical particles exhibit the highest values and the continuous composite has the least value for the volume fractions considered. This trend is similar to that observed for transverse modulus, as shown in figure 3.

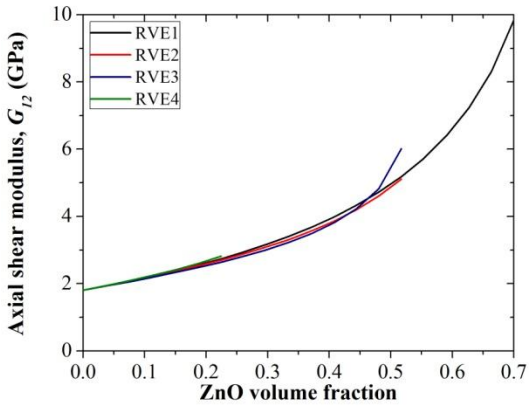

Figure 4. Variation of axial shear modulus as a function of volume fraction of ZnO

Figure 6 shows the effect of volume fraction on the Poisson's ratio ν_{12} for the different RVEs considered. While the continuous composite exhibits a monotonic increase in ν_{12} with an increase in volume fraction, the discontinuous composites with spherical and with ellipsoidal reinforcements show a decrease in ν_{12} for the ranges of volume fractions considered. For the discontinuous composite with cylindrical reinforcement, ν_{12} first decreases, reaches a minimum value at volume fraction of 0.4, and finally increases as the geometry tends towards a continuous composite at higher volume fractions.

Similar complex dependence of the Poisson's ratio ν_{23} on volume fraction of ZnO is shown in figure 7.

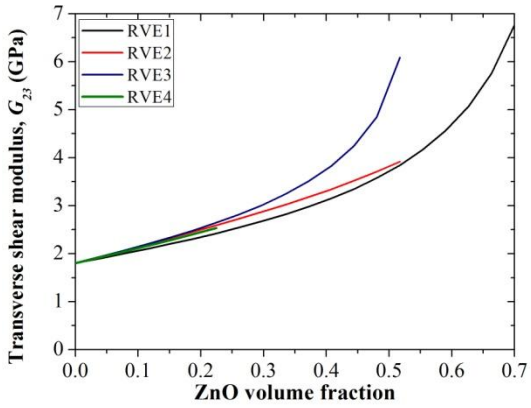

Figure 5. Variation of transverse shear modulus as a function of volume fraction of ZnO

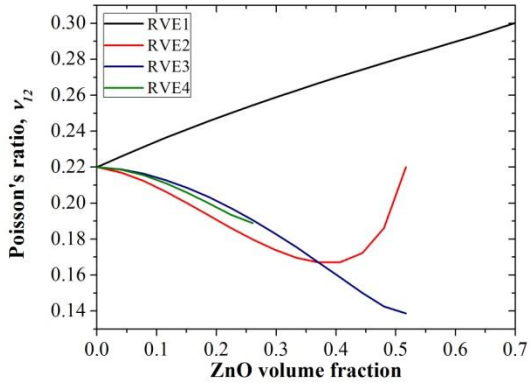

Figure 6. Variation of Poisson's ratio ν_{12} as a function of volume fraction of ZnO

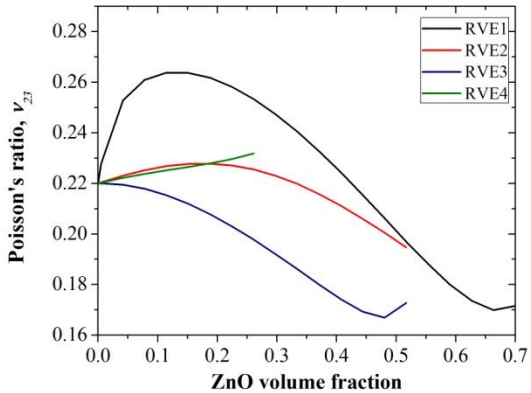

Figure 7. Variation of Poisson's ratio ν_{23} as a function of volume fraction of ZnO

6. Conclusions

COMSOL Multiphysics has been used to predict the effective elastic properties of SU8 photoresist reinforced with ZnO in various geometries. Representative volume elements for unidirectional continuous and discontinuous composites were defined in the form of a cube with edge length of 120 nm. Homogeneous displacement boundary conditions based on the symmetry of the RVEs were employed. Finite element analyses of the RVEs predict that continuous composites exhibit the maximum effective axial modulus and the maximum effective Poisson's ratios ν_{12} and ν_{23}, but the minimum effective transverse modulus and the minimum effective transverse shear modulus in the range of volume fractions of 0 - 0.52. The discontinuous composite with spherical reinforcement exhibits the minimum value in terms of the effective axial modulus, but the maximum values for effective transverse modulus and the effective transverse shear modulus, in the same range of volume fractions. Axial shear modulus is less sensitive to geometry and continuity of the reinforcements, compared to the other effective elastic properties. The discontinuous composites with ellipsoidal reinforcement have similar values as those with cylindrical reinforcements, especially at low volume fractions.

7. References

1. X. Wang, Piezoelectric nanogenerators-Harvesting ambient mechanical energy at the nanometer scale, *Nano Energy*, **1**, 13 - 24 (2012)
2. C. T. Sun, R.S. Vaidya, Prediction of composite properties using a representative volume element, *Composites Science and Technology*, **56**, 171 - 179 (1996)
3. A. Drago, M. J. Pindera, Micromechanical analysis of heterogeneous materials using FEMLAB, *Proceedings of the COMSOL Multiphysics User's Conference, Boston* (2005)
4. S. Li, General unit cells for micromechanical analyses of unidirectional composites, *Composites Part A*, **32**, 815 - 826 (2000)
5. S. Li, Boundary conditions for unit cells from periodic microstructures and their implications, *Composites Science and technology*, **68**, 1962 - 1974 (2008)
6. Y. Benveniste, A new approach to the application of Mori-Tanaka's theory in composite materials, *Mechanics of Materials*, **6**, 147 - 157 (1987)
7. L. V. Wang. *Photoacoustic Imaging and Spectroscopy*, CRC Press, Boca Raton (2009)
8. C. Jagadish C., S. J. Pearton, *Zinc Oxide Bulk, Thin Films and Nanostructures: Processing, Properties, and Applications*, Elsevier, Hong Kong (2006)

8. Acknowledgements

Financial support from the Department of Science and Technology - Science and Engineering Research Board (DST-SERB), Government of India, under Young Scientist Scheme (Grant No. YSS/2014/000830), and from Seed Grant, IIT Bhubaneswar (Grant No. SP062) are gratefully acknowledged.